PHYSICAL REVIEW E

STATISTICAL PHYSICS, PLASMAS, FLUIDS, AND RELATED INTERDISCIPLINARY TOPICS

THIRD SERIES, VOLUME 62, NUMBER 1 PART B JULY 2000

ARTICLES

Structure analysis of regenerated cellulose hydrogels by small-angle and ultra-small-angle x-ray scattering

Hitoshi Ando and Toshiki Konishi*

Central Laboratory, Rengo Company, Ltd., 186-1-4, Ohhiraki, Fukushima-ku, Osaka 553-0007, Japan

(Received 29 September 1999)

Absolute intensities $\Delta i(q)$ of small-angle x-ray scattering (SAXS) and ultra-small-angle x-ray scattering (USAXS) were measured in a wide range of scattering vector q from 2×10^{-4} to 0.5 Å^{-1} for transparent (VI-P) and translucent (VI-L) cellulose hydrogels prepared by coagulation and regeneration of viscose in acid solutions with and without acetone, respectively. We obtained the scattering intensities at very small q conveniently by desmearing the combined data measured by SAXS and USAXS. The plot of $\Delta i(q)q^2$ versus $\log_{10} q$ showed a peak at $-2.5<\log_{10} q<-1.0$. By assuming a two-phase model with the high-density phase (phase 1) composed of only cellulose and with the low-density phase (phase 2) composed of cellulose dispersed in water, volume fractions of phase 1 in VI-P and VI-L were determined to be 0.18 and 0.09, respectively, from the mean-square fluctuation of electron density determined as $\int \Delta i(q)q^2 dq$. By fitting the observed scattering profile with the theoretical particle scattering functions of spheres, the average diameter of the high-density region including crystallite was determined to be 120 Å for VI-P and 80 Å for VI-L. Similar analyses were applied also to freeze-dried VI-P. These results were consistent with those obtained by the wide-angle x-ray-diffraction measurement and also with the observation by scanning probe microscopy.

PACS number(s): 61.10.Eq, 82.70.Gg, 81.05.Lg

I. INTRODUCTION

The small-angle x-ray scattering (SAXS) method is one of the most useful techniques for studying the nanostructure of materials. However, in order to study samples with long-range higher-order structures such as polymer solids quantitatively, scattering intensity must be measured in a wide q range, where $q\,[=(4\pi/\lambda)\sin\theta]$ is the magnitude of the scattering vector, λ is the wavelength of the incident x ray, and 2θ is the scattering angle. Thus, the conventional Kratky type SAXS apparatus is not sufficient for the structure analysis of such samples, since it usually gives us reliable scattering intensity only in the range of $0.01<q<0.5\,\text{Å}^{-1}$ without using special equipment such as synchrotron radiation. To analyze the structure of such samples, the ultra-small-angle x-ray scattering (USAXS) apparatus, with which we can usually measure the scattering intensity for q down to $8\times10^{-5}\,\text{Å}^{-1}$ corresponding up to 8 μm in real space, is very useful. In this study, we applied these two techniques for regenerated cellulose hydrogels prepared by Saga and Saito [1].

The USAXS measurement and the data analysis are hindered by the low scattering intensity and the smearing effect. In order to overcome this problem, we used a convenient desmearing technique and determined the scattering function at $q<0.02\,\text{Å}^{-1}$ using the intense SAXS intensity.

We analyzed the SAXS and USAXS data in a very wide q range in the following two ways. First, we used the absolute scattering intensity to determine the invariant Q [2], which has been used also for (dry) regenerated cellulose fibers [3–5]. From Q, we can determine the volume fractions and concentrations of cellulose assuming a two-phase model. Second, we used the angular distribution of relative scattering intensity to estimate the size of component units by assuming that the gel sample is a particulate system and by fitting the profile with the theoretical particle scattering functions. We compared the results obtained by the SAXS and USAXS analyses with the wide-angle x-ray-diffraction (WAXD) measurement and with the observation by scanning probe microscopy (SPM). Furthermore, we discussed the effect of acetone which was added for the gelation of the transparent sample in the coagulation and regeneration agent. Finally, we compared the amorphous structure of our samples with that reported for fiber materials. Since our samples are

*Author to whom correspondence should be addressed.

regarded as precursors of dry elongated materials, such as a film and fiber, the investigation of the structure is important for improvement of regenerated cellulose materials.

II. EXPERIMENTAL SECTION

A. Samples

In this study, we used transparent and translucent cellulose hydrogels, VI-P and VI-L, respectively, for which details appear elsewhere [1]. The sample VI-P was obtained as follows; after a 1-mm-thick viscose (cellulose concentration: 9.5 wt. %) cast on a glass plate was coagulated and regenerated in a solution of 85 wt. % acetone and 0.5 N hydrochloric acid in water without elongation, it was desulfurized, bleached, and washed with water. The sample VI-L was obtained using the hydrochloric acid solution without acetone. The two samples were never allowed to dry. After substituting water by ethanol, and then by *t*-butanol in VI-P, the sample DVI-P was obtained by freeze-drying so as to minimize structural changes during the drying process.

The weight fractions of the cellulose in VI-P and VI-L were determined to be 0.39 and 0.19, respectively, by dry weight. The volume fraction of the total cellulose ν_{cell} in each sample was 0.28 for VI-P and 0.12 for VI-L. They were determined from the weight fractions and the reported density value for crystalline cellulose II $d_{\text{cell-II}}$ ($1.610\,\mathrm{g/cm^3}$) [6] for convenience sake. The volume fraction of the cellulose in DVI-P was 0.56, which was determined by dry weight from the volume [(area)×(thickness)] of the dry sample and the density of cellulose.

B. SPM

We observed the surface of DVI-P by SPM. Nano Scope IIIa Dimension 3000 (Digital Instruments Inc., Santa Barbara, CA) was employed in tapping mode with a probe of silicon cantilever (125 μm) at a drive amplitude of 1 V and scanning frequency of 1 Hz per line.

C. WAXD

The WAXD intensity was measured with a goniometer (CN2173C3, Rigaku Corporation, Tokyo, Japan) and an x-ray generator (CN4037B3, Rigaku Co., 50 kV–40 mA, wavelength $\lambda = 1.54\,\text{Å}$, Cu Kα) by a reflection method. Scattering from a standard amorphous sample prepared by saponification of cellulose triacetate was also measured. The data were corrected for the background intensity including that from water in the wet samples, for Lorentz factor, for absorption, and for polarization. The ratio χ_{cryst} of the weight of crystallite to the weight of the total cellulose in the sample was estimated from the peak area due to the $(1\bar{1}0)$, (110), and (200) diffractions from crystalline cellulose II and that from the amorphous part, whose scattering profile was assumed to be the same as that of the standard sample. Lateral crystallite sizes were calculated via the Scherrer equation [7], after the diffraction profiles without correction for the Lorentz factor were separated into the corresponding three peaks with the Lorentz function.

D. SAXS and USAXS

1. SAXS apparatus

A Kratky u-slit camera (Rigaku Co.) was employed in the SAXS measurements with a rotating anode x-ray generator (Rotaflex RU-300, Rigaku Co., 50 kV–280 mA, $\lambda = 1.54\,\text{Å}$, Cu Kα) and with a position-sensitive proportional counter (1024 channel) as a detector. For measurements of the two wet samples, we used a 1-mm-thick flat cell with Kapton windows in a vacuum-tight holder. We measured the scattering intensity from the two wet samples in the cell and from the dry sample in vacuum, and ''blank'' intensity from the cell filled with water for the wet sample and from the empty camera for the dry sample.

2. USAXS apparatus

The details of our USAXS apparatus have been described elsewhere [8]. It is composed of a Bonse-Hart (BH) camera [9] (Rigaku Co.) equipped with grooved single crystals of silicon and the same x-ray generator as used in the SAXS setup. The conditions of measurements for all the samples and blanks were the same as in the SAXS measurements. As the incident x-ray intensity, the intensity $I_{0,\mathrm{Ni}}$ transmitted through a nickel filter with 0.2-mm thickness was measured, before and after the USAXS measurements, and the average value was taken.

3. Desmearing

Here, we show data analyses using the SAXS data combined to the USAXS data, in order to obtain conveniently desmeared excess reduced scattering intensities $\Delta I_R(2\theta)$ as a function of the true scattering angle 2θ at very small angles from measured (smeared) excess reduced scattering intensities $\Delta \tilde{I}_R(2\tilde{\theta})$ as a function of an apparent scattering angle $2\tilde{\theta}$ [10]. $\Delta \tilde{I}_R(2\tilde{\theta})$ is given experimentally by

$$\Delta \tilde{I}_R(2\tilde{\theta}) = \tilde{I}_{R,\mathrm{sample}}(2\tilde{\theta}) - \tilde{I}_{R,\mathrm{blank}}(2\tilde{\theta}) \tag{1}$$

with

$$\tilde{I}_{R,i}(2\tilde{\theta}) = \frac{\tilde{I}_i(2\tilde{\theta})}{T_i I_{0,\mathrm{Ni},i}} \quad (i = \text{sample or blank}), \tag{2}$$

where $\tilde{I}_{\mathrm{sample}}(2\tilde{\theta})$ and $\tilde{I}_{\mathrm{blank}}(2\tilde{\theta})$ are smeared scattering intensities from the sample and blank, respectively, $I_{0,\mathrm{Ni,sample}}$ and $I_{0,\mathrm{Ni,blank}}$ are incident x-ray intensities transmitted through a 0.2-mm nickel filter in the measurements for the sample and blank, respectively, and T_{sample} and T_{blank} are transmittances for the sample and blank, respectively.

The relationships between the two scattering intensities $\Delta \tilde{I}_R(2\tilde{\theta})$ and $\Delta I_R(2\theta)$ for the USAXS apparatus (BH camera) and the SAXS apparatus (Kratky camera) are written as [11]

$$\Delta \tilde{I}_{R,\mathrm{BH}}(2\tilde{\theta}) = \int_{-\infty}^{\infty} \Delta I_R(2\theta)\, dy \tag{3}$$

with

$$2\theta = \sqrt{(2\tilde{\theta})^2 + y^2} \quad (\text{for BH camera}) \tag{4}$$

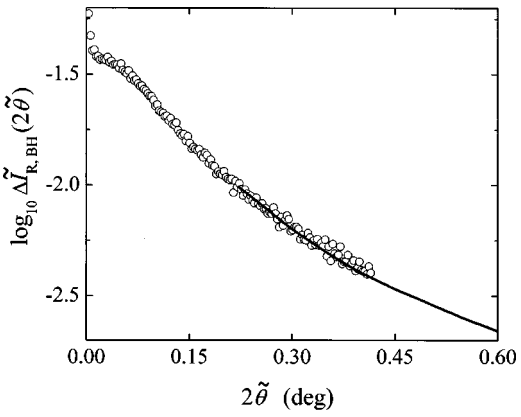

FIG. 1. $\log_{10}\Delta\tilde{I}_{R,\mathrm{BH}}(2\tilde{\theta})$ of VI-P with the SAXS and USAXS apparatuses; ——, the modified SAXS data; ○, the raw USAXS data.

and

$$\Delta\tilde{I}_{R,\mathrm{K}}(2\tilde{\theta})=k_{\mathrm{K}}\int_{-\infty}^{\infty}\int_{-\infty}^{\infty}W_{x,\mathrm{K}}(x)W_{y,\mathrm{K}}(y)\Delta I_R(2\theta)dx\,dy \tag{5}$$

with

$$2\theta=\sqrt{(2\tilde{\theta}-x)^2+y^2}\quad\text{(for Kratky camera)}, \tag{6}$$

where $\Delta\tilde{I}_{R,\mathrm{BH}}(2\tilde{\theta})$ and $\Delta\tilde{I}_{R,\mathrm{K}}(2\tilde{\theta})$ are smeared excess reduced scattering intensities for the BH and Kratky cameras, respectively, k_{K} is an apparatus constant including the difference in the optical systems between the BH and Kratky cameras, and $W_{x,\mathrm{K}}(x)$ and $W_{y,\mathrm{K}}(y)$ are the slit-width and slit-length weighting functions which can be obtained from the measured incident beam profile on the detector plane in the Kratky camera and the widths of detector slits. In Eq. (3), we assumed that the x-ray beam profile (weighting functions) in the USAXS apparatus is of infinite height and zero width. Solely from $\Delta\tilde{I}_{R,\mathrm{K}}(2\tilde{\theta})$ in the range of $0.2°\lesssim 2\theta\lesssim 9°$ measured with the SAXS apparatus, $k_{\mathrm{K}}\Delta I_R(2\theta)$ can be obtained in the range of $2\theta>0.25°$ by the method of Lake [12] and Schmidt and Hight [13] using Eq. (5) and the measured weighting functions. (Here, we note that the angular ranges given above and below hold only in the present case for the cellulose hydrogels, and they can vary depending on the scattering profile for the sample and also the accuracy of the scattering intensity required.)

On the other hand, in order to obtain $\Delta I_R(2\theta)$ in the range of $2\theta\lesssim 0.25°$, we need the USAXS data. In the determination of $\Delta I_R(2\theta)$ from $\Delta\tilde{I}_{R,\mathrm{BH}}(2\tilde{\theta})$ using Eq. (3) by the method of Guinier and Fournet [11], $\Delta\tilde{I}_{R,\mathrm{BH}}(2\tilde{\theta})$ at $2\tilde{\theta}$ ranging from 2θ to infinity is needed in principle. If we measure $\Delta\tilde{I}_{R,\mathrm{BH}}(2\tilde{\theta})$ only by the USAXS apparatus, it would take a long time because of low intensities especially at large angles. However, there is an alternative course to estimate $\Delta\tilde{I}_{R,\mathrm{BH}}(2\tilde{\theta})$ in the range of $2\theta\gtrsim 0.3°$, since $k_{\mathrm{K}}\Delta I_R(2\theta)$ has been obtained at the corresponding angles with the SAXS apparatus; because $k_{\mathrm{K}}\Delta\tilde{I}_{R,\mathrm{BH}}(2\tilde{\theta})$ can be derived by using Eq. (3) from $k_{\mathrm{K}}\Delta I_R(2\theta)$, we do not need to measure actually the USAXS intensity in this $2\tilde{\theta}$ range. We can obtain

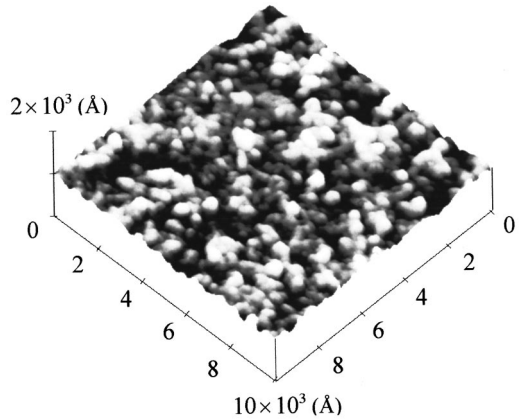

FIG. 2. The SPM image of the surface of DVI-P.

$\Delta I_R(2\theta)$ in the 2θ range smaller than 0.25° by desmearing the combined data composed of the modified data $k_{\mathrm{K}}\Delta\tilde{I}_{R,\mathrm{BH}}(2\tilde{\theta})$ measured with the SAXS apparatus in the range of $2\theta\gtrsim 0.3°$ and the raw data $\Delta\tilde{I}_{R,\mathrm{BH}}(2\tilde{\theta})$ measured with the USAXS apparatus in the range of $2\theta\lesssim 0.3°$, where k_{K} is determined in such a way that the data obtained in the above way connect smoothly. By this method, we can efficiently obtain x-ray scattering data in a very wide q range. Figure 1 shows that the two $\log_{10}\Delta\tilde{I}_{R,\mathrm{BH}}$'s obtained with the SAXS and USAXS apparatuses are consistent in the range of $0.25°<2\tilde{\theta}<0.4°$. (The data shown in Fig. 1 are for the sample VI-P.)

4. Absolute intensity

Next, we will evaluate the absolute intensity $\Delta i(q)$ [14], which is independent of the apparatus, from $\Delta I_R(q)$, which depends on the optical system. Using $\Delta i(q)$, we can calculate the *invariant* Q [2] which corresponds to the mean-square fluctuation of electron density $\langle\eta^2\rangle$, namely the scattering power, of a sample by the equation

$$Q\equiv\int_0^\infty\Delta i(q)q^2dq=\langle\eta^2\rangle. \tag{7}$$

For the two-phase systems, $\langle\eta^2\rangle$ is written in the form

$$\langle\eta^2\rangle=\phi_1(1-\phi_1)(\Delta\rho)^2, \tag{8}$$

where ϕ_1 is the volume fraction of phase 1 and $\Delta\rho$ is the electron density difference between phases 1 and 2 $(=\rho_1-\rho_2)$. $\Delta i(q)$ is experimentally obtained by the equation

$$\Delta i(q)=\frac{k}{l}\Delta I_R(q), \tag{9}$$

where k is the apparatus constant for the BH camera system and l is the thickness of the sample.

k was determined using measured SAXS and USAXS intensities $\Delta I_R(q)$ from colloidal silica particles, Cataloid SI-80P (average radius $\overline{R}=500$ Å, Catalyst & Chemicals Co., Ltd., Tokyo, Japan) in an aqueous dispersion containing 10^{-3} M sodium chloride as a standard, by Eqs. (7)–(9) with l determined to be 1.28 mm from the transmittance of the x ray through the dispersion, $\phi_1=0.0249$ by dry weight using

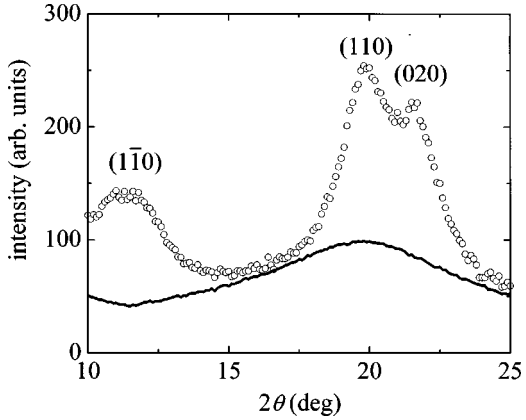

FIG. 3. WAXD of VI-P; ○, the VI-P data; ——, the amorphous data. Lattice planes of the crystal of cellulose II are indicated by Miller indices.

2.2 g/cm^3 as the density of silica, and the electron densities $\rho_1 = 1.10$ mol/cm^3 for the silica and $\rho_2 = 0.554$ mol/cm^3 for the dispersant.

III. RESULTS AND DISCUSSION

A. SPM

Figure 2 shows the SPM image of the surface of DVI-P. DVI-P is observed to be an assembly of particles, whose sizes are in the order of 10^2 Å as has been reported for regenerated cellulose membranes from cuprammonium hydroxide solution [16], although the size of the particle in the membranes was larger than that in our sample.

B. WAXD

The WAXD profile of VI-P resembled that of crystalline cellulose II as shown in Fig. 3. Other samples showed a similar profile. χ_{cryst}'s of VI-P, VI-L, and DVI-P were 0.3, 0.5, and 0.3, respectively. Lateral crystallite sizes calculated via the Scherrer equation from (1$\bar{1}$0), (110), and (020) reflections were 50 (±30) Å for all samples.

C. SAXS and USAXS

In Fig. 4(a), $\Delta i q^2$ for the three samples were plotted against $\log_{10} q$. The profile has two features. First, the profile shows a peak at $\log_{10} q \simeq -2.0$ for VI-P and DVI-P, and at $\log_{10} q \simeq -1.5$ for VI-L. Second, the profile at $\log_{10} q < -3.0$ for VI-L shows a distinct upturn, i.e., a steep increase in intensity with decreasing $\log_{10} q$, and that for DVI-P shows a weak upturn, while this is not the case for VI-P.

The appearance of the upturn, which is generally due to structures of larger dimension than a micron in the system, is consistent with the fact that VI-L is less transparent for visible radiation than VI-P for which upturn was hardly observed. The upturn for VI-L might have been caused by a scattering from pores which were actually observed to be about 2 μm by scanning electron microscopy for a cross section of a freeze-dried sample of VI-L [1]. The slight upturn observed for DVI-P may be attributed to a certain long-range inhomogeneity other than pores (see below), because pores were not observed.

The first feature invites some comments for the structural analyses using Eq. (7) from the data obtained at a finite range

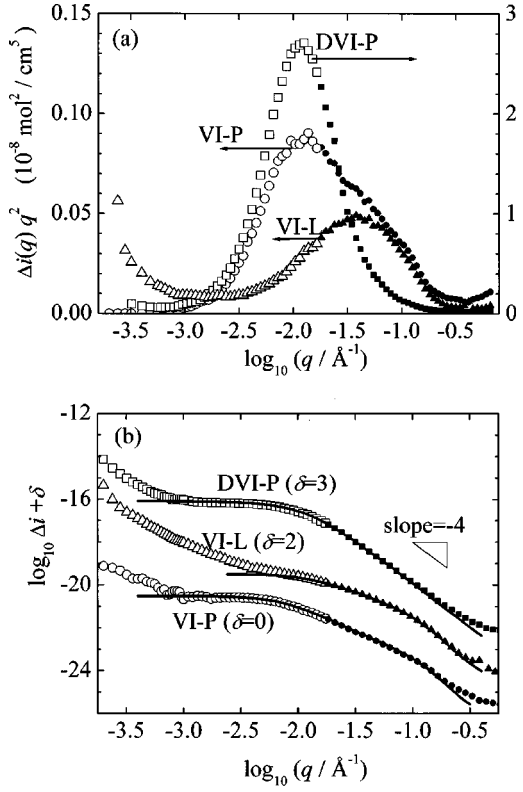

FIG. 4. (a) $\Delta i(q)\, q^2$ against $\log_{10} q$ of VI-P, VI-L, and DVI-P; ○ and ●, VI-P; △ and ▲, VI-L; □ and ■, DVI-P. Unfilled and filled symbols denote the data obtained with and without the USAXS data, respectively. Two different scales are used for the vertical axis; the scale on the left-hand side is for VI-P and VI-L, that on the right-hand side for DVI-P. (b) $\log_{10} \Delta i(q)$ against $\log_{10} q$ of VI-P, VI-L, and DVI-P shifted vertically by δ values shown in this figure; the symbols have the same meanings as those in (a); the inset triangle denotes the slope of −4. Solid curves denote the particle scattering functions of spheres calculated from Eq. (12) with the size distributions shown in Fig. 5.

of q at $-3.0 < \log_{10} q < -0.8$. First, the tail of the upturn does not affect the intensity for $\log_{10} q > -3.0$ very much, because the value of $\Delta i q^2$ at $\log_{10} q \simeq -3.0$ for all the samples is sufficiently low compared with the peak value (there is a minimum at $\log_{10} q \simeq -3.0$ in the profile for VI-L and DVI-P). Furthermore, in the double logarithmic plot [Fig. 4(b)] for all the samples, the slope at $\log q \simeq -0.8$ is almost −4, though leveling-off (larger slope than −4), which may be due to fine structures such as local cellulose chain structure and lattice structure of cellulose II, was observed at higher q at $\log_{10} q \gtrsim -0.8$. From these observations, it is reasonable, in the analyses of structures with 10–1000 Å, to assume that the value of $\Delta i q^2$ for $\log_{10} q < -3.0$ is zero and that the intensity for $\log_{10} q > -0.8$ follows Porod's law [$\Delta i(q) \propto q^{-4}$] [17].

The absolute scattering intensity $\Delta i(q)$ was used to obtain the invariant Q which corresponds to the mean-square fluctuation of electron density $\langle \eta^2 \rangle$ in the system. The value of Q was determined by Eq. (7) to be 0.010 for VI-P, 0.007 for VI-L, and 0.10 mol^2/cm^6 for DVI-P. We note that the data in the very small q range obtained with the USAXS apparatus shown by open symbols in Fig. 4(a) enabled us to evaluate Q correctly.

TABLE I. Cellulose concentration and volume fraction obtained through the analysis of the absolute intensities of USAXS and SAXS.

Sample	c_{cell}[a] (g cm^{-3})	ϕ_1[a]	ϕ_2[a]	ν_{cryst}[b]	ν_{am}[c]	ν_{disp}[a]
VI-P	0.2	0.18	0.82	(0.09)	0.09	0.10
VI-L	0.06	0.09	0.91	(0.06)	0.03	0.03
DVI-P	0.4	0.41	0.59	(0.16)	0.25	0.15

[a]Determined from the USAXS and SAXS data.
[b]Determined from the WAXD data.
[c]Determined from the USAXS, SAXS, and WAXD data.

Since Q has been experimentally obtained, the product $\phi_1(1-\phi_1)(\Delta\rho)^2$ can be determined from Eq. (8) if we assume a two-phase model. From the analysis using Q, Hermans *et al.* [3] showed the existence of air-filled voids in the fiber assuming a three-phase model consisting of crystalline regions, amorphous regions, and the voids, and Kratky and Miholic [4] studied a cluster of fibrils in the air-swollen fiber assuming a two-phase model consisting of fibrils and air-filled voids. One of the features of the gel samples used in this work compared with these fibers is that the dope of viscose is not elongated during sample preparation. Therefore, we expect that all cellulose molecules are not aggregated as fibrils. We assumed cellulose molecules except near crystalline regions dispersed uniformly all over the system. Thus, we employ the two-phase model, for convenience, where phase 1 is a high-density phase composed of only cellulose, which is crystalline and/or amorphous, and phase 2 is a low-density phase composed of water for the wet samples (or empty space for the dry sample) and cellulose dispersed in it. Then, we can obtain some structural parameters such as the weight fraction of the cellulose in the low-density phase f_L [=(weight of cellulose in phase 2)/(weight of total cellulose in the gel)] from $\phi_1(1-\phi_1)(\Delta\rho)^2$ and the volume fraction of the total cellulose ν_{cell} obtained by gravimetry.

According to the two-phase model, the electron density difference $\Delta\rho(f_L)$ is given by

$$\Delta\rho(f_L)=\rho_{cell}-\frac{\rho_{cell}\nu_{cell}f_L+\rho_{wa}(1-\nu_{cell})}{\nu_{cell}f_L+(1-\nu_{cell})} \quad \text{(for wet sample)}, \tag{10a}$$

$$\Delta\rho(f_L)=\rho_{cell}-\frac{\rho_{cell}\nu_{cell}f_L}{\nu_{cell}f_L+(1-\nu_{cell})} \quad \text{(for dry sample)}, \tag{10b}$$

where ρ_{cell} and ρ_{wa} are the electron densities of cellulose and water, respectively, and were calculated to be 0.854 and 0.554 mol/cm^3, respectively. $\phi_1(f_L)$ is given by

$$\phi_1(f_L)=\nu_{cell}(1-f_L). \tag{11}$$

Then, the value of f_L was determined from Q by Eqs. (7), (8), (10), and (11) to be 0.36 for VI-P, 0.25 for VI-L, and 0.27 for DVI-P. By using f_L, we calculated the cellulose concentration c_{cell} in phase 2 (the low-density phase) by $c_{cell}=(d_{cell\text{-}II}\nu_{cell}f_L)/(1+\nu_{cell}f_L-\nu_{cell})$. The values of c_{cell}, ϕ_1 calculated by Eq. (11), and ϕ_2 $(=1-\phi_1)$ are given in Table I.

Next, we tried to estimate the dimension of structures in the system by using the dependence of relative scattering intensity on the scattering angle (or q), while we did not use it in the previous analysis from Q but we used only the sum $(\int \Delta i q^2 dq)$. Here, we fit the measured scattering profile for $-2.5<\log_{10}q<-0.8$ with the theoretical particle scattering function [18] $P(qR)$ of a sphere with radius R taking its size distribution into consideration [19], where the existence of crystallites by WAXD and also the SPM observation may support the assumption of the particulate model. The theoretical value for $\Delta i(q)$ is written by the equation

$$\Delta i(q)\propto\int_0^\infty P(qR)R^3p(R)dR, \tag{12}$$

where $p(R)dR$ is the volume fraction of the particles with radii between R and $R+dR$ in the total volume of particles. The size distribution function was evaluated by using the program GNOM written by Svergun and Semenyuk [20]. The scattering profiles were reproduced by the theoretical values [solid curves in Fig. 4(b)] calculated with the size distributions shown in Fig. 5. The weight-average particle diameter was determined to be 120 for VI-P, 80 for VI-L, and 240 Å for DVI-P. The lateral crystallite size (about 50 Å) obtained from the WAXD data implies that the cellulose crystallite (the region with the highest density) is included in the particle assumed here and that the particles correspond to the high-density phase (phase 1) in the present two-phase model.

We note that, in the above analysis, we did not consider the effect of the interparticle interference, because this effect on the observed scattering profile is apparently smeared out except at very low angles when the size distribution of the particles is wide [21,22] as was shown for our systems in Fig. 5 [23].

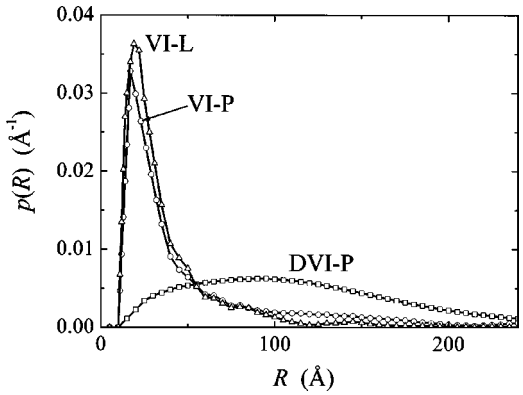

FIG. 5. Plots of the size distribution of the particle volume $p(R)$ of VI-P, VI-L, and DVI-P obtained by fitting the SAXS and USAXS data with the particle scattering functions of spheres shown in Fig. 4(a). ○, VI-P; △, VI-L; □, DVI-P.

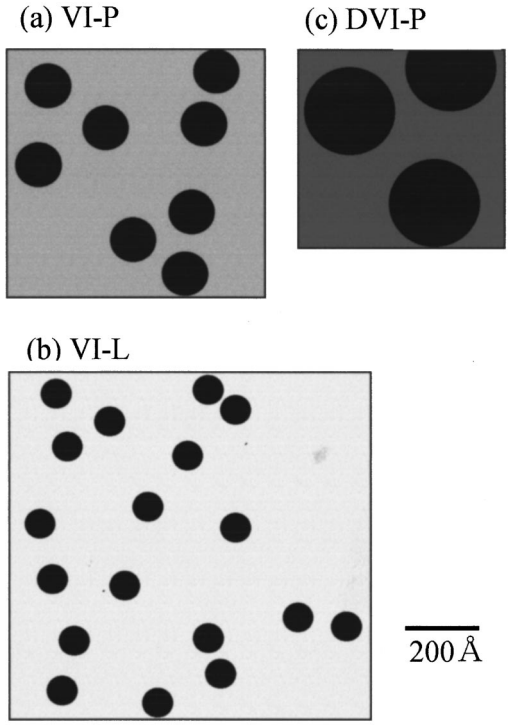

FIG. 6. Schematic structures of the two-phase particulate system for (a) VI-P, (b) VI-L, and (c) DVI-P through the analysis of the absolute intensities of SAXS and USAXS; ●, high-density particle with weight-average diameter; all the samples have the same amount of cellulose; the gradation of the shade reflects the cellulose concentration.

From the structural parameters obtained above through the analysis using Q and the particle size analysis, schematic structures of the two-phase particulate system are shown in Figs. 6(a) for VI-P, (b) for VI-L, and (c) for DVI-P. Only the particles with the weight-average diameter are shown. Each picture for all the samples was drawn so as to include the same amount of cellulose and the gradation of shade reflects the cellulose concentrations.

Here, we consider the effect of acetone at the gelation by comparing the two cases in its presence and absence in the regeneration solution, namely VI-P [Fig. 6(a)] and VI-L [Fig. 6(b)]. The cellulose concentration is higher, and the size of the high-density particle is larger in VI-P than in VI-L. These results may be attributed to the presence of acetone at the gelation. Since acetone is expected to have less affinity for cellulose than water, acetone may increase the concentration of the cellulose in the dope to allow the cellulose molecules to aggregate more efficiently. This effect may reduce the long-range inhomogeneity in the resultant gel to make the VI-P sample transparent.

Next, we note the effect of drying from the comparison of Figs. 6(a) and 6(c). Considering that the total volume of phase 1 (or $\phi_1/\nu_{\mathrm{cell}}$) for VI-P did not significantly change by drying, the difference in the average diameter may be explained by aggregation of a few particles in VI-P into a bigger one in DVI-P. This size and the number density of the particles in DVI-P after the drying as shown in Fig. 6(c) are not inconsistent with the SPM image (Fig. 2). It is also noted that the slight upturn observed in the USAXS profile for DVI-P at $\log_{10}q < -3.0$ in Fig. 4(a) may be attributed to a long-range inhomogeneity formed by shrinkage due to drying.

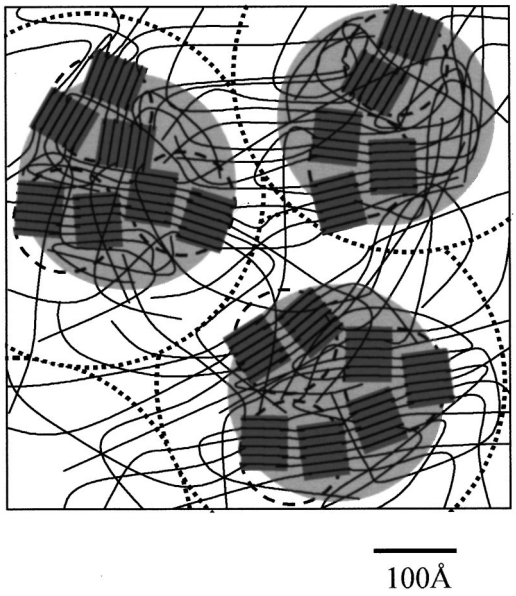

FIG. 7. A schematic picture of DVI-P based on the results of USAXS, SAXS, WAXD, and SPM. ——, cellulose chain; dark shadowed area, crystalline region; light shadowed area, high-density phase; ···, particle observed by SPM; — — —, high-density phase in VI-P.

Finally, in order to compare the amorphous structure of our dry sample DVI-P with that reported for fiber materials, Fig. 7 was obtained by modification of Fig. 6(c) to include cellulose chains by taking the results of SPM and WAXD into consideration. In drawing Fig. 7, we considered the values of the volume fractions of cellulose in the crystalline region ν_{cryst} $(=\nu_{\mathrm{cell}}\chi_{\mathrm{cryst}})$, in the amorphous region ν_{am} $[=\nu_{\mathrm{cell}}(1-f_L-\chi_{\mathrm{cryst}})]$ in phase 1, and in the disperse region ν_{disp} $(=\nu_{\mathrm{cell}}f_L)$ in phase 2. In Table I, these values are shown with those for VI-P and VI-L. The structure of the crystalline region has been investigated in detail, and the lattice structure and lattice constants thoroughly determined [6], but the studies of the structure of the amorphous region in regenerated cellulose materials are still developing [25–27]. Schurz and Lenz [25] inferred that there were, in the fiber, an amorphous region which connected successive crystallites lengthwise in elementary fibrils and another kind of region which connected laterally adjacent elementary fibrils. These regions are expected to have different characteristics; e.g., the orientation and density of the cellulose in the former is higher than that in the latter. In our case, we concluded that the cellulose in our regenerated cellulose hydrogel, except for that in the crystalline region, was divided into two regions, i.e., the high-density amorphous region near the crystalline region and the low-density phase where local cellulose segments were dispersed in water as shown in Fig. 7. Considering that our samples were not elongated, the high-density phase in our gel may serve as a precursor of the elementary fibril in the elongated fiber and the amorphous region in the high-density phase in our gel may correspond to the amorphous region inside the elementary fibril in the sample of Schurz and Lenz [25].

ACKNOWLEDGMENTS

The authors would like to express their sincere thanks to Dr. Norio Ise, Director, Central Laboratory, for valuable discussions and for his help in preparing the manuscript, to Hiroshi Saga and Hidenao Saito, Fukui Research Laboratory, for the preparation of the samples and helpful discussions, and to Dr. Dmitri I. Svergun, European Molecular Biology Laboratory and Russian Academy of Sciences, for the GNOM software.

[1] H. Saga and H. Saito, US Patent No. 5,962,005 (1999); H. Saga and H. Saito (unpublished).

[2] G. Porod, in *Small Angle X-ray Scattering*, edited by O. Glatter and O. Kratky (Academic, London, 1982).

[3] P. H. Hermans, D. Heikens, and A. Weidinger, J. Polym. Sci. **35**, 145 (1959).

[4] O. Kratky and G. Miholic, J. Polym. Sci., Part C: Polym. Symp. **2**, 449 (1963).

[5] J. Schurz, J. Lenz, and E. Wrentschur, Angew. Makromol. Chem. **229**, 175 (1995).

[6] F. J. Kolpak and J. Blackwell, Macromolecules **9**, 273 (1976).

[7] P. Scherrer, Göttinger Nachrichten **2**, 98 (1918).

[8] T. Konishi, N. Ise, H. Matsuoka, H. Yamaoka, I. S. Sogami, and T. Yoshiyama, Phys. Rev. B **51**, 3914 (1995).

[9] U. Bonse and M. Hart, Z. Phys. **189**, 151 (1966).

[10] The apparent scattering angle $2\tilde{\theta}$ is the angle between central lines of the incident beam and the scattered x-ray beam detected.

[11] A. Guinier and G. Fournet, *Small Angle Scattering of X-Rays* (Wiley, New York, 1955).

[12] J. A. Lake, Acta Crystallogr. **23**, 191 (1967).

[13] P. W. Schmidt and R. Hight, Acta Crystallogr. **13**, 480 (1960).

[14] Strictly speaking, the absolute intensity defined here is different from the generally employed [(scattering intensity)/(incident intensity)] (see O. Kratky, Ref. [15]), and is the product of the ratio with $r^2/(2\pi^2 I_e V N_A^2)$ with I_e being the Thomson factor, r the distance between the sample and detector, V the scattering volume, and N_A the Avogadro number, for convenience.

[15] O. Kratky, in *Small Angle X-ray Scattering*, edited by O. Glatter and O. Kratky (Academic, London, 1982).

[16] H. Iijima, M. Iwata, M. Inamoto, and K. Kamide, Polym. J. (Tokyo) **29**, 147 (1997).

[17] G. Porod, Kolloid-Z. **124**, 83 (1951).

[18] L. Rayleigh, Proc. R. Soc. London, Ser. A **84**, 25 (1911).

[19] Since the shape of the cellulose crystallite, for example in the elongated fiber, is reportedly not spherical but rather rodlike, it may be more precise to fit the data by theoretical values for rods or ellipsoids. However, the particles in our gel systems are expected to be less rodlike, because our samples were not elongated in the preparation, and we thought it not highly realistic to do such a detailed analysis with the rod model at this stage of study because the real system may be composed of particles with a very wide size distribution and with wide distribution of electron density. Thus, we just discussed the size distribution in terms of equivalent spheres.

[20] D. I. Svergun, A. V. Semenyuk, and L. A. Feigin, Acta Crystallogr. **44**, 244 (1988); D. I. Svergun, J. Appl. Crystallogr. **24**, 485 (1991).

[21] P. van Beurten and A. Vrij, J. Chem. Phys. **74**, 2744 (1981).

[22] G. G. Long, S. Kraueger, P. R. Jemian, D. R. Black, H. E. Burdette, J. P. Cline, and R. A. Gerhardt, J. Appl. Crystallogr. **23**, 535 (1990).

[23] In fact, when we consider the interparticle structure function represented by a hard-sphere interaction potential (Ref. [24]) with the value of ϕ_1 and the size distribution shown in Fig. 5, the weight average diameters are calculated to be 150, 80, and 400 Å for VI-P, VI-L, and DVI-P, respectively. Though the values for VI-P and DVI-P are larger than those obtained without considering the interparticle interference, the discrepancy does not affect the conclusions.

[24] A. Vrij, J. Chem. Phys. **71**, 3267 (1979).

[25] J. Schurz and J. Lenz, Macromol. Symp. **83**, 273 (1994).

[26] C. Yamane, M. Mori, M. Saito, and K. Okajima, Polym. J. (Tokyo) **12**, 1039 (1996).

[27] E. Togawa and T. Kondo, J. Polym. Sci., Part B: Polym. Phys. **37**, 451 (1999).